

## Alternatively Spliced Exon B of Myosin Va Is Essential for Binding the Tail-Associated Light Chain Shared by Dynein<sup>†</sup>

Zsuzsa Hódi,<sup>‡</sup> Attila L. Németh,<sup>‡</sup> László Radnai,<sup>‡</sup> Csaba Hetényi,<sup>‡</sup> Katalin Schlett,<sup>§</sup> Andrea Bodor,<sup>||</sup> András Perczel,<sup>⊥</sup> and László Nyitrai<sup>\*‡</sup>

Departments of Biochemistry, Physiology and Neurobiology, Theoretical Chemistry, and Organic Chemistry, Eötvös Loránd University, Budapest, Hungary

Received May 18, 2006; Revised Manuscript Received July 31, 2006

**ABSTRACT:** A 10 kDa dynein light chain (DLC), previously identified as a tail light chain of myosin Va, may function as a cargo-binding and/or regulatory subunit of both myosin and dynein. Here, we identify and characterize the binding site of DLC on myosin Va. Fragments of the human myosin Va tail and the DLC2 isoform were expressed, and their complex formation was analyzed by pull-down assays, gel filtration, and spectroscopic methods. DLC2 was found to bind as a homodimer to a ~15 residue segment (Ile1280–Ile1294) localized between the medial and distal coiled-coil domains of the tail. The binding region contains the three residues coded by the alternatively spliced exon B (Asp1284–Lys1286). Removal of exon B eliminates DLC2 binding. Co-localization experiments in a transfected mammalian cell line confirm our finding that exon B is essential for DLC2 binding. Using circular dichroism, we demonstrate that binding of DLC2 to a ~85 residue disordered domain (Pro1235–Arg1320) induces some helical structure and stabilizes both flanking coiled-coil domains (melting temperature increases by ~7 °C). This result shows that DLC2 promotes the assembly of the coiled-coil domains of myosin Va. Nuclear magnetic resonance spectroscopy and docking simulations show that a 15 residue peptide (Ile1280–Ile1294) binds to the surface grooves on DLC2 similarly to other known binding partners of DLCs. When our data are taken together, they suggest that exon B and its associated DLC2 have a significant effect on the structure of parts of the coiled-coil tail domains and such a way could influence the regulation and cargo-binding function of myosin Va.

Class V myosins are involved in the short-range intracellular transport of vesicles and molecules mostly in the actin-rich cortical region of the cell (for a review, see ref 1). They are processive actin-based motors moving by a “hand-over-hand” mechanism along actin filaments (2, 3). Mammalian genomes contain three myosin V heavy-chain genes: MYO5A, MYO5B, and MYO5C. Mutations of MYO5A are responsible for the *dilute* phenotype and Griscelli syndrome type 1 in mice and humans, respectively (4, 5). Myosin Va (myoVa)<sup>1</sup> is composed of two heavy chains, six calmodulins (one or two could be substituted by essential light chains) associated with the neck region, and a 10 kDa light chain, originally identified as a light chain of dynein (called DLC;

alternative names are LC8, DLC8, and PIN) bound to the tail region (6, 7). The tail region contains coiled-coil dimerizing domains interrupted with noncoiled-coil regions and a C-terminal globular tail domain (GTD) involved in cargo binding (8, 9). At least six isoforms of myoVa are expressed, partially tissue specifically, by alternative splicing of three exons (exons B, D, and F) in the tail region. An isoform that is expressed abundantly in the brain includes only exon B, while a mainly melanocyte-specific isoform includes exons D and F (10–12). Exon F together with GTD was found to bind to melanosomes via the adaptor protein melanophilin (13–15). An isoform containing only exon D associates with vesicles near the Golgi area (16). No function for exon B has been assigned thus far. The regulation of the ATPase and the motor activity of myoVa are thought to be achieved by Ca<sup>+2</sup> binding to the calmodulin (CaM) subunits and folding back the globular tail domain toward the heads (17–21).

DLC was first described as a light-chain component of the *Chlamydomonas* outer dynein arm and later a component of mammalian flagellar and cytoplasmic dyneins (22, 23). In the multisubunit cargo-binding tail region of the dynein motor, it is associated with the intermediate chain (24). DLC is a highly conserved protein, with >90% sequence identity between any two orthologues (7, 25). Mammalian species contain two DLC genes (DYNLL1 and DYNLL2; the proteins referred to here as DLC1 and DLC2). DLCs were found to bind to a diverse array of proteins and even to RNAs

<sup>†</sup> This work was supported by OTKA (Hungarian Scientific Research Fund) Grants T43746, K61784, TS049812, TS044711 (to L.N.), and T46994 (to A.P.).

\* To whom correspondence should be addressed: Department of Biochemistry, Eötvös Loránd University, Pázmány P.s. 1/c, Budapest, Hungary, H-1117. Telephone: 36-1381-2171. Fax: 36-1381-2172. E-mail: nyitrai@cerberus.elte.hu.

<sup>‡</sup> Department of Biochemistry.

<sup>§</sup> Department of Physiology and Neurobiology.

<sup>||</sup> Department of Theoretical Chemistry.

<sup>⊥</sup> Department of Organic Chemistry.

<sup>1</sup> Abbreviations: CaM, calmodulin; CD, circular dichroism; DBD, DLC2 binding domain of myosin Va; DSS, sodium 4,4-dimethyl-4-silapentane-1-sulphonate; GFP, green-fluorescent protein; GST, glutathione-S-transferase; myoVa, myosin Va; nNOS, neuronal nitric oxide synthase; PBS, phosphate-buffered saline; rmsd, root-mean-square deviation; TFE, trifluoroethanol; TCEP, tris(2-carboxyethyl)phosphine; β-ME, 2-mercaptoethanol.

besides the two motor proteins, such as the neuronal nitric oxide synthase (nNOS) enzyme (26, 27), I $\kappa$ B $\alpha$  (28), bicoid mRNA via the swallow protein (29, 30), PTH mRNA (31), GKAP and gephyrin postsynaptic scaffolding proteins (32–34), Bim and Bmf “BH3-only” proapoptotic proteins (35, 36), p53-binding protein 1 (37), several virus proteins (38, 39) and possibly many other proteins (40, 41). Mutations of DLC cause apoptotic cell death in *Drosophila* (42). On the basis of the above properties, it was hypothesized that DLCs function as a cargo adapter of myoVa and dynein motors in intracellular transport and/or sequestration; moreover, as soluble proteins, they have additional function(s) in eukaryotic cells (26, 34, 43). Recent results suggest that DLC can also function as a tumor promoter by supporting cell survival through p21-activated kinase-dependent phosphorylation (44). Reports originally showed that DLC1 and DLC2 bound equally to both motors and that both isoforms were identified as light chains of isolated cytoplasmic dynein complexes (25, 34). However, recent studies indicated that *in vivo* DLC1 and DLC2 bind to dynein and myoVa, respectively (35, 36). Crystal and NMR structures of DLC1 were determined both in the apo form and in complex with short binding peptides of nNOS and Bim, respectively (43, 45). The solution structure of DLC2 is also known (35). DLC forms a homodimer with 2-fold symmetry. A five-stranded  $\beta$  sheet and two  $\alpha$  helices are arranged in a novel fold. Four strands of the  $\beta$  sheet from each monomer and the fifth strand from the other monomer form the core, while the two pairs of  $\alpha$  helices cover the outer faces of the dimer. Two deep hydrophobic target binding grooves are formed at the two edges of the  $\beta$  sheet; the target peptides were found to bind as antiparallel  $\beta$  strands extending the central  $\beta$  sheets.

Here, we report that the three residues of the alternatively spliced exon B of the myoVa tail is part of the binding site of DLC2 within a disordered domain between the medial and distal coiled-coil regions of the tail. Importantly, binding of DLC2 induces some folding of its binding domain and stabilizes the flanking coiled-coil domains, promoting the assembly of the two heavy chains. Molecular docking and nuclear magnetic resonance (NMR) spectroscopic studies indicate that the myoVa-binding peptide occupies the same surface groove as other known binding partners of DLC2. Binding of the DLC2 dimer to the dimeric heavy chain is likely asymmetric, allowing for a third partner, a cargo, or regulatory protein to interact with the motor complex. Preliminary results of this work have been reported (46).

## MATERIALS AND METHODS

**Expression and Purification of DLC2 and myoVa Fragments.** Human DLC2 (Uniprot accession number Q96FJ2) was obtained from human brain cDNA by the RevertAid First cDNA synthesis kit (Fermentas). A human pancreas cDNA library (Stratagene) was used as a template in polymerase chain reaction (PCR) reactions to generate several myoVa constructs (numbering as in Q9Y4I1-2): MV-(1244–1442), MV2(1158–1368), M1(1244–1386), M11-(1244–1368), M11 $\Delta$ B(1244–1368,  $\Delta$ 1284–1286), M2-(1307–1442), M3(1244–1316), M4(1244–1284), M6(1275–1316), M7(1275–1297), M7 $\Delta$ B(1275–1297,  $\Delta$ 1284–1286), and M8(1294–1316). The myosin isoforms thus obtained have an exon pattern in the alternatively spliced tail region: ABCEG (10). One isoform containing exon D (ACDEG)

was cloned independently from human Jurkat cell cDNA: M1 $\Delta$ B+D(1244–1395) (numbering as in Q9Y4I1-1). The PCR products were cloned into pGEX4T-1 (Amersham) and/or pET15b (Novagen) vectors using *Bam*HI/*Nde*I and *Eco*RI. Constructs were transformed in BL21(DE3)pLysS or BL21-(DE3) “Rosetta” (Novagen) cells. After induction, cells were grown at 37 °C for 3 h in 2YT medium (except for NMR spectroscopy in minimal media containing <sup>15</sup>NH<sub>4</sub>Cl). Glutathione-S-transferase (GST)-fusion and His-tagged proteins were purified on glutathione Sepharose (Amersham) and Ni<sup>2+</sup>-affinity columns (Novagen), respectively. The His-tagged proteins were digested by thrombin and further purified on HiTrapQ ion-exchange column chromatography (Amersham). The protein concentration was determined using UV spectroscopy, by measuring the absorbance at 280 nm using calculated molar extinction coefficients (47) or by a modified Lowry method (48).

**Peptide Synthesis.** The DLC2-binding peptide of myoVa (IQPKDDKNTMTDSTI) was synthesized in-house by standard solid-phase techniques using Fmoc chemistry. The DLC-binding nNOS peptide (EMKDTGIQVDRL) was a kind gift of Dr. Rodriguez-Crespo.

**Analytical Gel-Filtration Chromatography.** MyoVa constructs, DLC2, and their complexes were analyzed by gel-filtration chromatography using Superdex 200 HR 10/30 and 75 HR 10/30 columns (Amersham) in 150 mM NaCl, 20 mM Tris, and 0.5 mM dithiothreitol (DTT) at pH 7.6 and 4 °C with a 0.5 mL/min flow rate. Absorbances were detected at 220 and 280 nm by a LKB VWM2141 photometer (Pharmacia). Apparent molecular mass of the proteins were estimated using low-molecular-weight standards (Amersham).

**GST Pull-Down Assay.** For direct binding experiments, the soluble phases of *Escherichia coli* cell lysates containing GST–myosin fragments were incubated first with DLC2 and then with glutathion-Sepharose beads for 30 min in phosphate-buffered saline (PBS) buffer containing 2 mM 2-mercaptoethanol ( $\beta$ -ME) at 25 °C. The pellets were washed twice with the same buffer and eluted with reduced glutathion. For direct competitive binding experiments, the GST–M7–DLC2 complex-bound beads were mixed with a DLC2-binding peptide of nNOS successively at 1:1, 10:1, and 100:1 molar ratios in PBS. The remaining DLC2 was eluted from the beads and resolved along with other samples on 15% tricine sodium dodecyl sulfate–polyacrylamide gel electrophoresis (SDS–PAGE) as in ref 49.

**Native Gel Electrophoresis.** Complex formation between myoVa constructs and DLC2 was studied by native PAGE prepared similarly to SDS–PAGE but without SDS. A constant concentration of a myoVa construct (7–12  $\mu$ M) was incubated for 30 min with an increasing amount of DLC2 (molar ratio from 1:0.125 to 1:4) in 150 mM NaCl, 20 mM Tris, and 2 mM  $\beta$ -ME at pH 7.6. Samples were run on 12–15% PAGE on ice. Band intensities were quantitated after Coomassie Brilliant Blue staining with Genetools software (SynGene). Binding stoichiometry was estimated from plotting peak areas of the complex against the ratio of the two proteins. Because it was only the complex that migrated as a sharp band, the apparent dissociation constant was determined by fitting a plot of the fraction saturation versus the total DLC2 concentration.

**Transfection and Co-localization.** NE-4C, a mouse neuroectodermal stem cell line (50) was used for transfection assays. Cells were cultivated in minimum essential medium (Sigma) supplemented with 4 mM glutamine, 5% fetal calf serum (Merck), and 40  $\mu\text{g}/\text{mL}$  gentamycin (Sigma). For transient transfections,  $7.5 \times 10^4$  cells were seeded onto poly-L-lysine (Sigma) coated 13 mm diameter glass coverslips in 24 well plates. The next day after seeding, cells were transfected with plasmid constructs using Lipofectamine 2000 reagent (Invitrogen). The constructs used for the transfection assays were as follows: human DLC2 and myoVa tail fragments (from residues Ala1244 to the C-terminal Val, either containing the tail exon B or not; exons D and F were absent in these constructs) were cloned into both pEGFP-C1 and pDsRed2-N1 vectors (Clontech) in frame with the respective fluorescence proteins. A total of 1  $\mu\text{g}$  of plasmid was used for single transfection experiments, while in cotransfection assays, 0.5  $\mu\text{g}$  of green-fluorescent protein (GFP)-tagged DLC2 was combined with 1.5  $\mu\text{g}$  of DsRed-tagged myosin constructs (or vice versa). In all cases, 2  $\mu\text{L}$  of Lipofectamine 2000 was used for each microgram of plasmid per well. Growth medium was replaced 6 h after the transfection, and cells were grown for an additional 18 h and then fixated by 4% paraformaldehyde in PBS at pH 7.4 for 20 min at room temperature. Nuclei were labeled by DRAQ5 for 10 min (1/2000 dilution; BioStatus Ltd.), and then coverslips were washed and mounted using Mowiol 4.88 (Polysciences). Confocal microscopy was carried out using an Olympus IX71 microscope equipped with a 60 $\times$  oil immersion objective, 488 nm argon, 546 and 633 nm helium–neon lasers, and FluoView500 software. A sequential scanning mode was used during recordings to completely rule out potential cross-talk between channels.

**Structure Predictions.** COILS and PAIRCOIL were used to predict coiled-coil regions in the myoVa tail. PONDR (51) and GlobProt (52) were applied to search for unstructured regions. Secondary-structure predictions were performed by the PHD server (53).

**Limited Proteolysis.** Limited proteolysis of the myoVa constructs M1, MV2, M3 (20–60  $\mu\text{M}$ ), myoVa fragment–DLC2 complexes (1:2 molar ratio), and DLC2 alone were performed at either 0 or 20  $^\circ\text{C}$  with trypsin (1:100 weight ratio to the myosin fragment) and proteinase K at 25  $^\circ\text{C}$  (1:400 weight ratio) in 150 mM NaCl, 20 mM Tris-HCl, and 2 mM  $\beta$ -ME at pH 7.6. The proteolyzed fragments were blotted to a nitrocellulose membrane and analyzed by N-terminal peptide sequencing.

**Circular Dichroism (CD) Spectroscopy.** CD spectra were recorded on a JASCO J720 spectropolarimeter equipped with a Neslab RTE-111 temperature controller using a 1 mm cuvette and wavelength range between 190 and 250 nm. The DLC2 spectra were subtracted from that of the myoVa fragment–DLC2 complexes. All measurements were performed in 20 mM phosphate buffer at pH 7.6 containing 150 mM NaCl and 0.5 mM DTT at 15–30  $\mu\text{M}$  protein concentrations. For thermal denaturation experiments, protein samples were heated at a constant 1  $^\circ\text{C}/\text{min}$  rate and the CD signal was monitored at 220 nm. Curves were analyzed for a two-state transition between the folded dimer (D) and unfolded monomers (M). Dissociation/unfolding constant,  $K_d = [\text{M}]^2/[\text{D}]$ , is defined by

$$K_d = 2C_{\text{tot}}f_M^2/(1/f_M) \quad (1)$$

$C_{\text{tot}}$  is the total protein concentration, and  $f_M$  is the fraction of the monomeric chain. The measured ellipticity per residue depends upon  $f_M$  according to

$$\theta_{\text{obs}} = f_M[\theta_M - \theta_D] + \theta_D \quad (2)$$

$\theta_M$  and  $\theta_D$  are ellipticity per residue of the monomer and dimer, respectively.  $\theta_D$  was assumed to depend linearly upon the temperature and was calculated from  $\theta_D = \theta_{D_0} + \alpha T$ , where  $\theta_{D_0}$  is the hypothetical ellipticity at 0 K and  $\alpha$  is a constant.  $K_d$  is a function of the temperature and total protein concentration

$$K_d = C_{\text{tot}} \exp\{\Delta H(1/T_{\text{mobs}} - 1/T)\}/R \quad (3)$$

$\Delta H$  is the van't Hoff enthalpy of unfolding at the transition midpoint temperature  $T_{\text{mobs}}$ , where  $f_M = 0.5$ , and  $R$  is the gas constant. The difference in heat capacity between the unfolded monomers and the native dimers is assumed to be small and could be neglected (54). Equations 1–3 were applied for nonlinear curve fitting. After  $\Delta G$  and  $\Delta S$  were determined from  $\Delta G = -RT \ln K$  and  $\Delta G = \Delta H - \Delta S$ , the melting temperature ( $T_m$ ) at  $\Delta G = 0$  ( $K_d = 1$ ) was calculated (54). Concentration dependence studies were carried out by monitoring the molar ellipticities at 222 nm (using cuvettes with light paths from 1 mm to 1 cm). Curves were fitted assuming a two-state monomer–dimer transition. Data for trifluoroethanol (TFE) experiments were acquired after 5 min of incubation of the samples with 50 vol/% vol TFE. To estimate secondary-structure elements, deconvolution of the spectra was performed using CDSSTR at the Dichroweb server (55). Helical content was also estimated as described in ref 56.

**NMR Spectroscopy.** All measurements were performed on a Bruker DRX500 spectrometer equipped with a  $z$ -gradient 5 mm triple-resonance probe head at 300 and 310 K. Temperature values were checked with the 1,2-ethanediol calibration method. Chemical shifts were referenced to an external sodium 4,4-dimethyl-4-silapentane-1-sulphonate (DSS) standard.  $^1\text{H}$ ,  $^{15}\text{N}$  heteronuclear single-quantum coherence (HSQC) spectra of  $^{15}\text{N}$ -labeled DLC2 in free form and complexed to a synthetic myoVa peptide representing the DLC binding sequence (IQPKDDKNTMTDSTI) were acquired by the fastHSQC pulse program using the WATERGATE sequence for water suppression. Sequential backbone resonance assignments for the unbound DLC2 were obtained from the 3D HNCA, HN(CO)CA, and C(CO)NH correlation measurements performed on the double-labeled  $^{15}\text{N}$ ,  $^{13}\text{C}$  DLC2 sample, partly by a comparison with data obtained by Day et al. (35). Spectra were processed by XWIN-NMR (Bruker AG) and NMRPipe (57) software packages and analyzed by XEASY. The  $^{15}\text{N}$ -labeled DLC2 and the myoVa-binding peptide were dissolved in 20 mM NaCl, 0.04% Na–azide, 20 mM sodium phosphate buffer at pH 7.6, 2 mM tris(2-carboxyethyl)phosphine (TCEP), and a 9:1  $\text{H}_2\text{O}/\text{D}_2\text{O}$  ratio. The protein concentration was kept at  $\sim 1.0$  mM. Stepwise titration with the myoVa peptide (concentration of the stock solution was 18 mM) was performed up to a 1:1.25 protein/ligand ratio. The complex was subsequently titrated with adding a DLC-binding nNOS peptide (EMKDT-

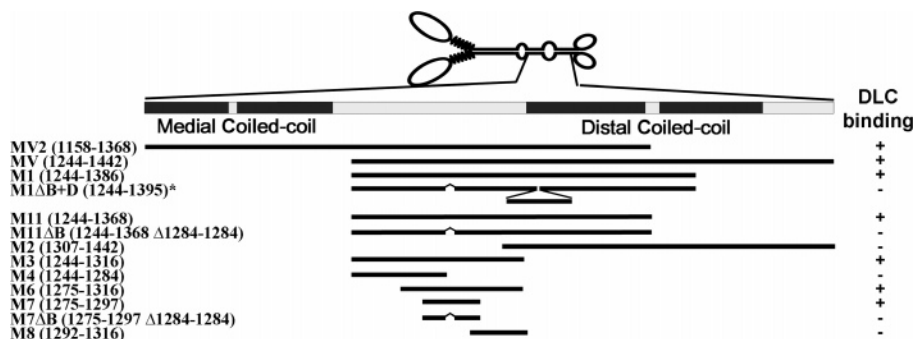


FIGURE 1: Schematic diagram of various recombinant myoVa constructs and their sequence positions used in this work. The tail of myoVa is divided into proximal, medial, and distal coiled-coil domains, separated by the PEST sequence and another (~85 residue) noncoiled-coil domain, respectively. The globular tail domain follows the distal coiled-coil region. Coiled-coil and noncoiled-coil regions are represented by black and gray boxes. Note that both the medial and distal coiled-coil domains have a short discontinuity. “+” and “-” signs on the right indicate binding or nonbinding to DLC2. (\*) Sequence numbering in M1ΔB+D (a fragment containing exon D but not exon B) is according to the melanocyte-specific myoVa isoform (Uniprot: Q9Y4I1-1), while all of the other numberings are of the brain-specific isoform (Q9Y4I1-2).

GIQVDRL; stock concentration of 18 mM) to the same molar excess as the myoVa peptide.

**Molecular Docking.** The structure of the complex between DLC1 and a DLC-binding nonapeptide of Bim (MSCDK-STQT; PDB access code 1F95) (45) was used in the modeling studies. It is noteworthy that the structure of the DLC2–Bmf peptide complex (Bmf and Bim are homologous BH-3-only proteins) was found to be very similar to the above complex (35). Minimization of the complex in explicit water surroundings was done by GROMACS (58). The ligand position of the energy-minimized complex was reproduced using AutoDock 3.0 (59) at 3.1 Å root-mean-square deviation (rmsd) calculated for the central CDKST pentapeptide part. (This rmsd is acceptable considering that the original PDB 1F95 structure was an energy-minimized average NMR structure and the ligand is quite large.) Details of the docking procedure are described in our previous work (60). In the present study, the size of the grid box was 50 × 50 × 100 points with 0.375 Å grid spacing. A total of 100 docking runs were performed for three peptides: myoVa-binding peptide Ac-PKDDKNTMTD-NMe, myoVa peptide lacking the exon B sequence Ac-QPKNTMTD-NMe, and the Bim peptide. Differences in binding affinities of the ligand molecules were estimated from the intermolecular interaction energies (61). Note that, because of the high computational demand of the docking simulations, shorter peptides had to be used for docking compared to those for the NMR experiments.

## RESULTS

**Identification of the DLC2 Binding Site on the myoVa Tail by *In Vitro* Pull-Down Assay and Size-Exclusion Chromatography.** The tail region of class V myosins can be divided into three predicted coiled-coil domains interrupted by noncoiled-coil segments and followed by the cargo-binding globular tail domain (62). In our nomenclature, as schematically illustrated in Figure 1, the proximal coiled-coil domain (residues Arg903–His1104) starts just after the calmodulin-binding neck domains and ends at the calpain-sensitive PEST site (residues Val1105–Lys1159). The medial (Leu1150–Asp1234) and distal (Leu1321–Val1419) coiled-coil domains are separated by a ~85 residue noncoiled-coil region (residues Pro1235–Arg1320). Note that part of this region

(Arg1248–Val1263) shows a low probability (~0.5) of coiled-coil formation, and a secondary-structure prediction reveals peptide stretches with high α-helical propensity. The coiled-coil prediction breaks down for a short stretch of peptide in both the medial (around Pro1195) and distal (around Pro1365) coiled-coil domains. Prediction programs were applied to see if the noncoiled-coil segment is able to form a globular domain or rather represent an intrinsically unstructured domain of the myoVa tail. PONDR (51) predicted that the whole region except for the last couple of residues is more likely unfolded than folded. On the other hand, GlobProt (52) using different definitions predicted that it is only a short stretch of peptide (Pro1282–Met1289) that may not fold into any stable secondary structure.

Previous yeast two-hybrid experiments showed that DLC2 binds between residues 1236–1420 of the tail region of brain-specific myoVa (34). The identified myoVa isoform has an alternatively spliced exon pattern of ABCEG (10, 11). We have produced overlapping truncated recombinant myoVa tail fragments (Figure 1) and used analytical gel filtration and GST pull-down assays to further narrow the DLC2 binding site on the heavy chain. Construct MV corresponds to the yeast two-hybrid clone. A longer fragment (MV2) was also designed to check the effect of a N-terminal extension of the binding region (also comprising a coiled-coil segment) on the DLC2–myoVa interaction. Construct M1ΔB+D contains exon D but not exon B. Because recent results had shown that the DLC2 isoform binds to myoVa *in vivo* (35, 36), we used this paralogue throughout this work.

Analytical gel filtration was employed to show interactions between DLC2 and the myoVa tail fragments. DLC2 formed complexes with the MV and M1 fragments but not with the M2 fragment (data not shown). GST pull-down assays (Figure 2) show that DLC2 binds robustly to GST–M3, GST–M6, and GST–M7. M7 consists of 23 residues with amino acid sequence SQKEAIQPKDDKNTMTDSTILLE. Because this peptide contains the alternatively spliced exon B (underlined), we have made two constructs without exon B (M7ΔB and M11ΔB). DLC2 binding of GST–M7ΔB was tested by the pull-down assay (Figure 2), while that of M11ΔB was checked by analytical gel filtration and compared to M11 (Figure 3). The fragments lacking exon B did not show any interaction with DLC2, thus strongly suggesting

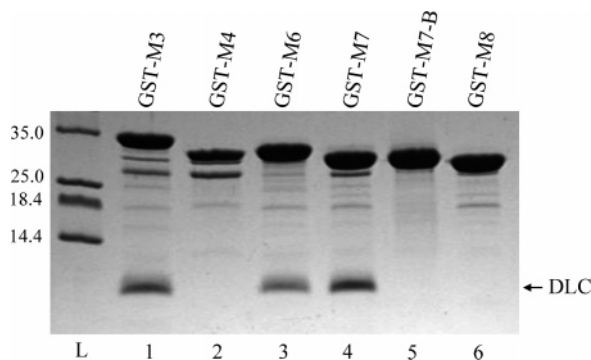


FIGURE 2: Mapping of the DLC2 binding site in myoVa by a GST pull-down assay. Coomassie-blue-stained SDS-PAGE showing the interactions between various GST-myovA constructs and DLC2. Cell lysates containing GST-M1, GST-M3, GST-M4, GST-M6, GST-M7, GST-M7 $\Delta$ B, and GST-M8 were incubated with DLC2 (2.5  $\mu$ M) and 15  $\mu$ L of glutathione Sepharose beads in 2 mL of PBS buffer and 2 mM  $\beta$ -ME at room temperature and then after washing 3 times with PBS eluted from the beads by reduced glutathione and loaded on SDS-PAGE.

that exon B is part of the DLC2 binding site and is essential for binding. Human DLC2 runs as a dimer (apparent molecular mass of 21 kDa) by size-exclusion chromatography under the conditions used (see the globular molecular-weight markers in Figure 3B), and dissociation to monomers could be observed only at pH 4 in accordance with previous results (63). Densitometric analysis of the bands on SDS-PAGE of DLC2-MV and DLC2-M11 complexes (compared to known amounts of the individual components) shows a stoichiometry of 1:1; i.e., one DLC2 dimer binds to one myovA heavy-chain dimer (inset of Figure 3A). It is noteworthy that the elution volume of the myovA tail constructs compared to globular marker proteins has a considerably higher apparent molecular weight than globular proteins of similar sizes. The construct M1 $\Delta$ B+D did not pull-down DLC2, indicating that isoforms containing exon D instead of exon B do not bind the tail light chain (data not shown). When the above results were summarized, progressive truncation led to the narrowing of the DLC2 binding region to a  $\sim$ 15 residue continuous peptide segment of the myovA heavy chain between residues Ile1280 and Ile1294.

Binding of DLC2 to the myovA tail fragments was confirmed by native gel electrophoresis (Figure 4A). Titration of M11 with DLC2 shows saturation at 1:1 stoichiometry, providing further evidence that one DLC2 dimer binds to one myosin dimer (Figure 4B), corroborating the densitometric analysis of DLC2 on tissue-purified myovA (6). Fitting densitometric data to a single binding site equation results in a dissociation constant of  $\sim$ 0.4  $\mu$ M. Higher complexes did not appear even in the presence of high excess DLC2, suggesting that one DLC2 dimer likely bridges the two heavy chains. The same results were obtained with MV2. M3, a monomeric myovA tail construct, also showed saturation binding to DLC2 with the expected stoichiometry of two M13 monomers bound to one DLC dimer.

*DLC2 Binding to Exon B of myovA in Vivo as Revealed by Confocal Microscopy.* The interactions between GFP-tagged DLC2 and DsRed-tagged myovA fragments with and without exon B were tested in NE-4C cells, a mouse neuroectodermal stem cell line (50). For these experiments,

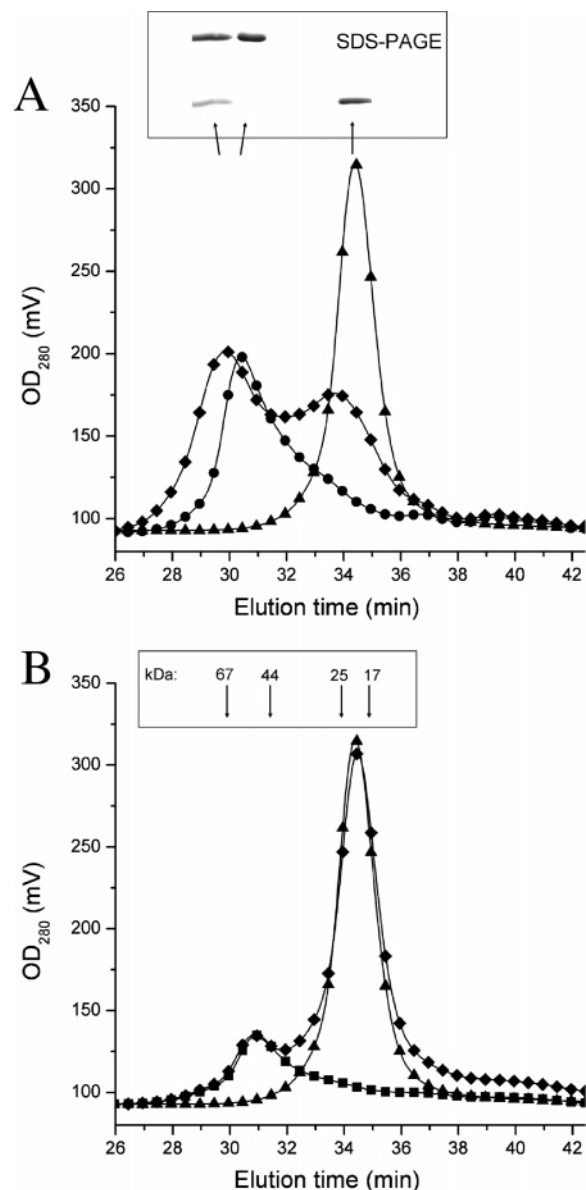


FIGURE 3: Analytical gel filtration showing the interactions between myovA tail fragments and DLC2. (A) Recombinant DLC2 alone (▲), M11 alone (●), and a mixture of M11 and DLC2 (◆) and (B) DLC2 (▲), M11 $\Delta$ B alone (■), and a mixture of M11 $\Delta$ B and DLC2 (◆) were loaded (5  $\mu$ M M11, 3  $\mu$ M M11 $\Delta$ B, and 7  $\mu$ M DLC) on a Superdex 200 HR 10/30 column in 150 mM NaCl, 20 mM Tris, and 0.5 mM DTT at pH 7.6 and 4  $^{\circ}$ C with a 0.5 mL/min flow rate. Absorbances were detected at 280 nm. The inset on A is a SDS-PAGE of the three indicated peaks (arrows) from the chromatogram of the M11-DLC2 complex and M11 alone. Arrows in B above the chromatogram indicate molecular-weight markers in kilodaltons.

we used a myovA tail construct containing the globular tail domain. In single transfections, GFP-tagged DLC2 was found evenly distributed in transfected cells, while both DsRed-tagged myovA constructs formed patches (possibly aggregates) in the cytoplasm (data not shown). Cotransfection of GFP-DLC2 together with DsRed-myovA lacking exon B led to similar expression patterns: GFP-DLC2 remained evenly distributed within the cell, even in those places where its expression overlapped with large patches of DsRed-myosin (Figure 5). A strikingly different GFP-DLC2 distribution was observed when cells were cotransfected with exon B containing DsRed-myovA: GFP-DLC2 formed

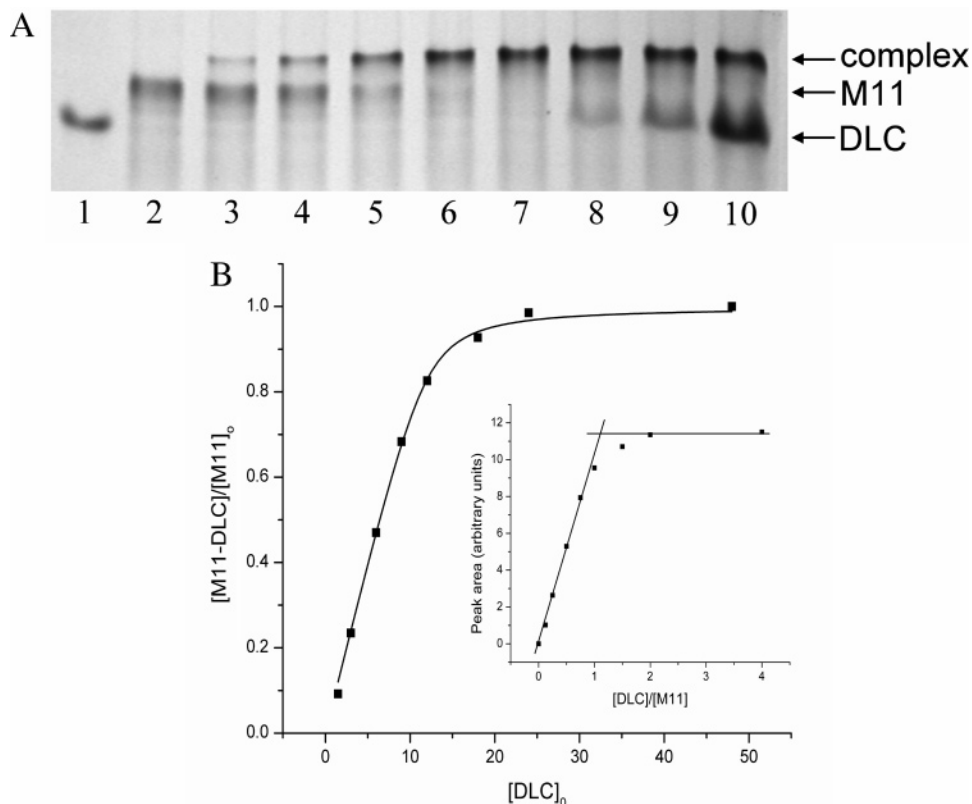


FIGURE 4: Native gel electrophoresis of the complex formation between DLC2 and myoVa fragments. (A) Titration of a constant concentration of M11 (12  $\mu$ M) with DLC2 in 150 mM NaCl, 20 mM Tris, and 2 mM  $\beta$ -ME at pH 7.6 monitored by native PAGE on ice. Lanes 1 and 2, DLC2 (12  $\mu$ M) and M11 alone; lanes 3–10, mixtures of M11 and DLC2 at molar ratios: 1:0.125, 1:0.25, 1:0.5, 1:0.75, 1:1, 1:1.5, 1:2, and 1:4. (B) Apparent dissociation constant was estimated by fitting data points from a plot of the fraction saturation (average of two gels) versus the total DLC2 concentration ( $K_d = 0.4 \pm 0.05 \mu$ M). The inset in B is a plot of the intensities of the bands corresponding to the complex as a function of the molar ratios of M11 and DLC2. Intersection of the two slopes to the abscissa yields a stoichiometry of 1 mol of DLC2 bound to 1 mol of M11. The bands of the complex were analyzed by the Genetools quantification software (SynGene).

patches that highly co-localized with DsRed–myoVa patches in the cytoplasm (Figure 5). Exon B containing DsRed–myoVa was less prone to make large patches (aggregates) when it was cotransfected with GFP–DLC2, indicating the stabilization of the dimer tail region in the presence of DLC2. When the transfection experiments with mammalian cells were taken together, they corroborated our *in vitro* finding that DLC2 could interact with the myoVa tail only if exon B was expressed.

**DLC2 Globally Protects the Tail Domains against Limited Proteolysis.** The structural effect of DLC2 binding to myoVa fragments was studied by limited tryptic and proteinase K digestion (Figure 6). DLC2 is highly stable against limited proteolysis at the enzyme/substrate ratio used for the experiment. M1 alone (18 kDa) was degraded into smaller fragments, while a  $\sim$ 16 kDa fragment was clearly protected in the presence of 2-fold molar excess DLC2. The protected fragment has the same N-terminal sequence as M1, indicating that residues were cleaved off the C-terminal region (likely at residue Arg1396). Thus, DLC2 protected tryptic cleavage sites near and remote from its binding site, suggesting a global stabilizing effect on the myosin tail. The constructs M11 and M11 $\Delta$ B were designed on the basis of the limited proteolysis results, and they did not contain the proteolytically sensitive C-terminal residues of M1. In the case of MV2, both coiled-coils were partially protected in the presence of DLC2 and a shorter stable fragment was produced with the N terminus at Gly1198, suggesting that

the stabilizing effect of DLC2 applies to both flanking coiled-coil domains. The identified cleavage sites within the medial and distal coiled-coil domains, respectively, are located at the coiled-coil breaks (see above). The broad specificity proteinase K gave qualitatively similar results. It degraded MV2 to many fragments but at significantly slower rates in the presence of DLC2. The fragments that were protected by DLC2 binding ( $\sim$ 14.5,  $\sim$ 16.5, and  $\sim$ 19.5 kDa) were analyzed by N-terminal sequencing. On the basis of the sequences and the size of the peptides, the DLC2-protected sites were identified at or near Ala1199 (next to a site that was also protected from tryptic digestion), Val1274, and Leu1326. We conclude that DLC2 stabilizes myoVa fragments and globally protects the tail domains around its binding site from proteolytic digestion.

**CD Spectroscopy Shows That DLC2 Binding Stabilizes Its Binding Domain and the Flanking Coiled-Coil Domains.** The effect of DLC2 binding on the secondary structure of myoVa fragments was monitored by CD spectroscopy (Figure 7). The far-UV CD spectrum of human DLC2 is similar to that reported previously for *Drosophila* DLC (63), typical of an  $\alpha/\beta$  protein (Figure 7A). The spectrum of a representative of the myoVa fragments (MV2) is shown in Figure 6A and is typical for an  $\alpha$ -helical coiled-coil protein with double minima at 208 and 222 nm and a ratio of  $\theta_{222}/\theta_{208}$  close to 1 (64). Calculated helical contents of M11, M2, and MV2 at room temperature are  $\sim$ 20%,  $\sim$ 45%, and  $\sim$ 42%, respectively. The spectra of the DLC2-bound myoVa fragments

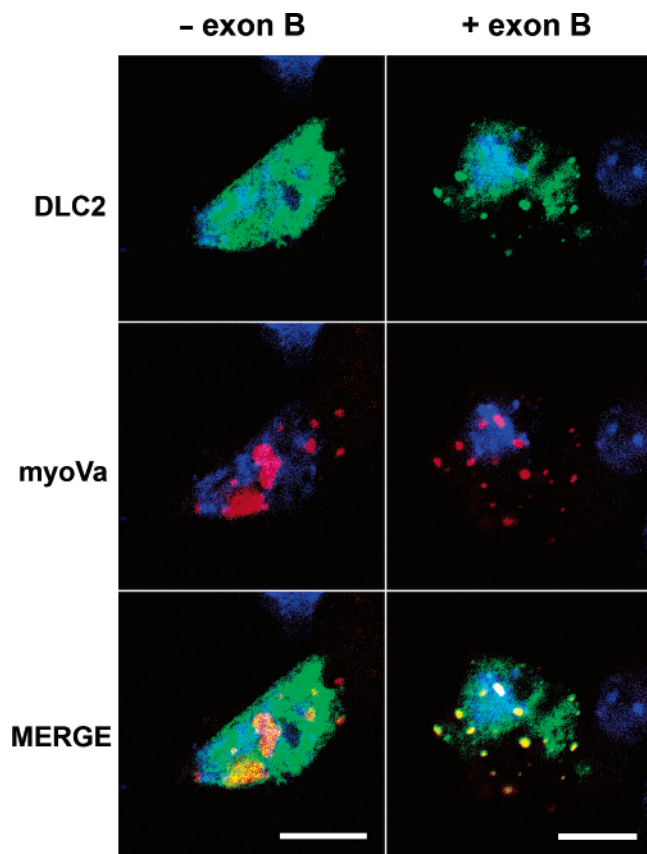


FIGURE 5: Co-localization of DLC2 and myoVa tail constructs in a mouse neuroectodermal cell line (NE-4C). Exon B containing myoVa tail fragment (including the medial and distal coiled-coil domains as well as the globular tail domain but without alternative exons D and F) recruits DLC2 in NE-4C cells. Single-section confocal images taken from cotransfected cells with GFP-DLC2 and DsRed-myoVa without exon B (left column) or GFP-DLC2 and DsRed-myoVa containing exon B (right column). The presence of exon B changes GFP-DLC2 distribution as exon B recruits DLC2 to the expressed myoVa. Overlap of the DLC2 (green) and myoVa (red) signals appears yellow in the merged picture. Nuclei were labeled by DRAQ5 (blue). Bars represent 10  $\mu\text{m}$ .

were generated by subtracting the DLC2 spectrum from that of the complex. A 10% increase in  $\alpha$  helix in the case of M11 but no change in the similarly obtained spectrum of M11 $\Delta$ B was observed. The increase in the calculated helical content of M11 could correspond to  $\sim$ 13 residues folded into the  $\alpha$  helix upon DLC2 binding, assuming that there is no change in the secondary structure of DLC2 upon complex formation. The latter assumption is based on the fact that the apo- and peptide-bound DLC structures are superimposable (45). In the case of the MV2-DLC2 complex,  $\alpha$ -helix content increased by 4% (Figure 7A), indicating that  $\sim$ 10 residues gained  $\alpha$ -helical structure. The spectrum of MV2 was also recorded in the presence of 50% TFE, a substance known to promote  $\alpha$ -helix formation in peptide chains with high helix propensity (65). The molar ellipticity increased at 222 nm, and the  $\theta_{222}/\theta_{208}$  ratio shifted well below 1, indicating uncoiling of MV2 into single  $\alpha$  helices (Figure 7A).

The stability of the myoVa fragments and their DLC2 complexes was investigated by thermal denaturation, monitoring the ellipticity change at 222 nm. Spectral changes were accompanied by a decrease in the  $\theta_{222}/\theta_{208}$  ratio and an isodichroic point at 203 nm, consistent with a two-state

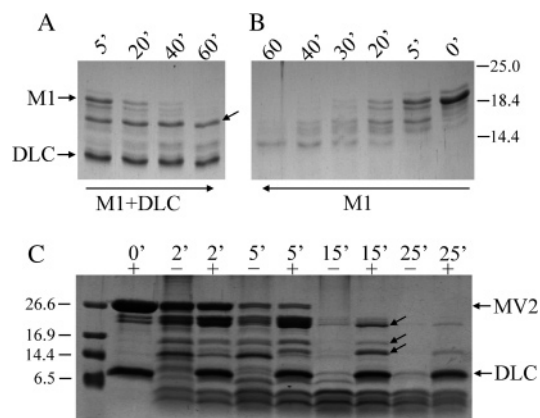


FIGURE 6: Limited proteolysis of myoVa fragments. (A) Limited tryptic digestion of M1 (10  $\mu\text{M}$ ) preincubated with DLC (1:1.5 molar ratio) and (B) M1 alone were performed in 150 mM NaCl, 20 mM Tris, and 2 mM  $\beta$ -ME at pH 7.6 and 0  $^{\circ}\text{C}$  with a 1:100 weight ratio of enzyme/myoVa fragment. Samples in the lines represent the proteolytic fragments after 5–60 min of digestion and 0 min as a control. (C) Proteinase K digests of MV2 in the presence and absence of DLC performed at 25  $^{\circ}\text{C}$  with a 1:400 weight ratio of enzyme/myoVa fragment. Lanes show the proteolytic fragments after 0–60 min with (+) and without (–) DLC. DLC is stable against digestion with both proteases under the conditions used. Arrows points to DLC2-protected fragments, which were analyzed by N-terminal sequencing.

coiled-coil dimer/random coil monomer transition upon heating. All myoVa fragments became denatured at relatively low temperature (20–40  $^{\circ}\text{C}$ ), indicating a relatively low stability of the coiled-coil dimers (parts C and D of Figure 7). Thermal unfolding of the myoVa fragments were essentially reversible as expected for coiled-coil dimers. The assumption that the myoVa fragments denature in a two-state cooperative transition between a folded dimer and an unfolded monomer was verified by showing that there was no concentration dependence of the  $T_m$  values evaluated at  $\Delta G = 0$  (see the Materials and Methods). The average  $T_m$  of MV2 at equilibrium was  $58.7 \pm 0.7$   $^{\circ}\text{C}$  over a range of 4–64  $\mu\text{M}$  (Table 1). DLC2 unfolded at a much higher temperature (72  $^{\circ}\text{C}$ ). At this value, the tail fragments were already completely unfolded (Figure 7C). The pretransition linear shift seen in the temperature-dependent ellipticity of MV2 (Figure 7C) is likely associated with fraying at the coiled-coil ends (66). Upon the addition of DLC2, the thermal denaturation temperature of myoVa fragments significantly increased. The difference between the observed melting temperature of M11 ( $T_{\text{mobs}} = 21.4$   $^{\circ}\text{C}$ ) and that of the M11-DLC2 complex was 7.3  $^{\circ}\text{C}$ . On the other hand, upon the addition of DLC2 to the M11 $\Delta$ B fragment, no such shift was observed. This experimental result proves that the shift in thermal stability of M11 is the consequence of complex formation and that exon B is essential for the interaction (Figure 7C). MV2 alone ( $T_{\text{mobs}} = 36.0$   $^{\circ}\text{C}$ ) shows a higher thermal stability than M11 presumably because of its extra coiled-coil sequence at the N terminus. DLC2 shifts the melting temperature by 4.8  $^{\circ}\text{C}$ . Table 1 shows the observed melting temperatures of the myoVa fragments in the absence and presence of DLC2 together with van't Hoff unfolding enthalpies and dimer dissociation constants. MV2 forms a fairly stable dimer at micromolar concentration and room temperature both in the absence ( $K_d = 29$  nM) and presence ( $K_d = 4$  nM) of DLC2; however, at 37  $^{\circ}\text{C}$ , it forms a weak

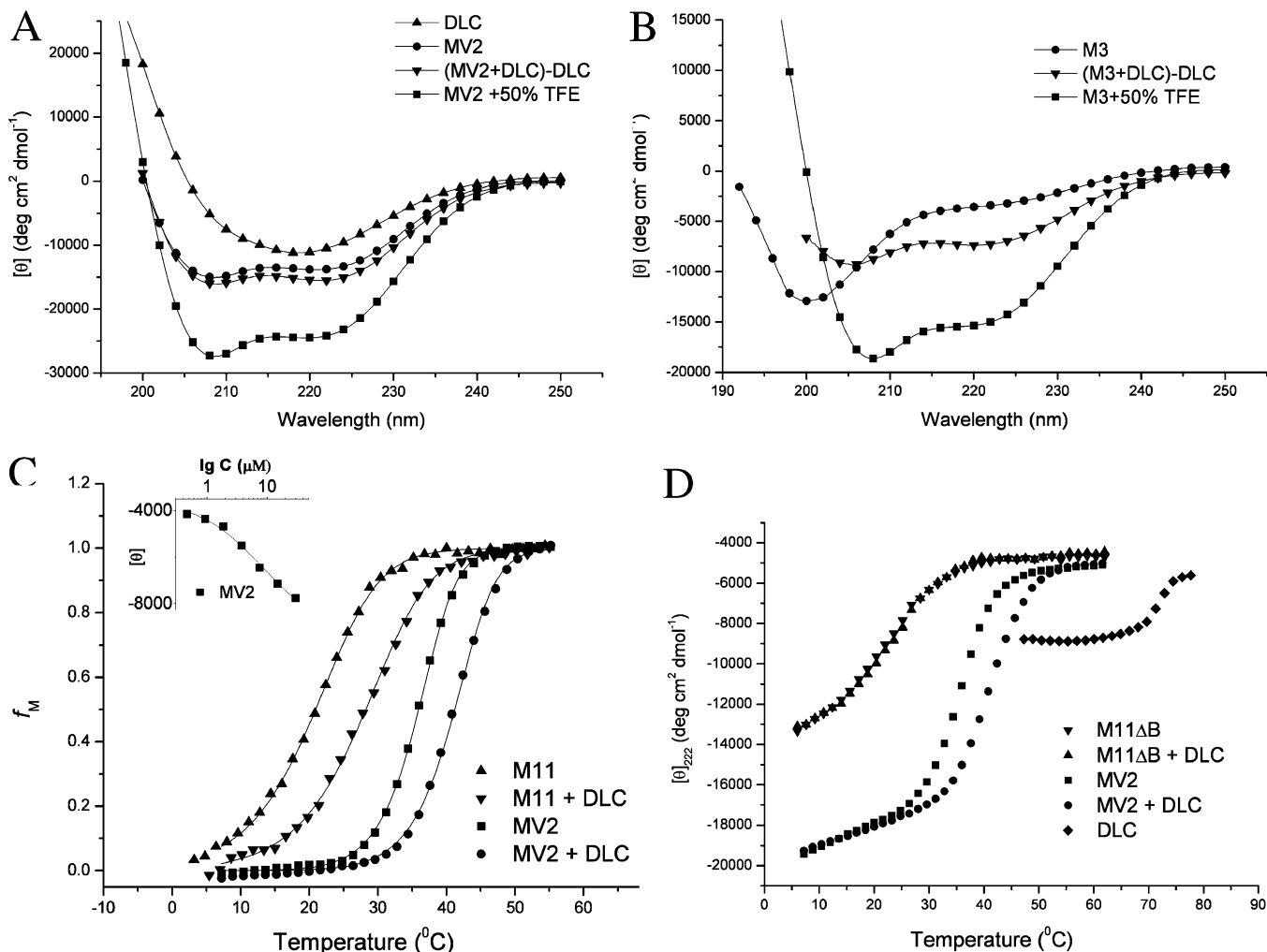


FIGURE 7: CD spectroscopy of myoVa constructs and their complexes with DLC2. (A) Far-UV spectra of DLC2 (▲), MV2 (●), the complex of MV2 and DLC2 after the subtraction of the DLC2 spectrum (▼), and MV2 in the presence of 50% TFE (■) were recorded at 16  $\mu$ M monomer concentration in 20 mM phosphate buffer at pH 7.6 containing 150 mM NaCl and 0.5 mM DTT at 25 °C. (B) Far-UV spectra of M3 (●), the complex of M3 and DLC2 after the subtraction of the DLC2 spectrum (▼), and M3 in the presence of 50% TFE (■) were recorded at 30  $\mu$ M protein concentration as in A. (C) Thermal unfolding profiles of M11 (▲), the M11–DLC2 complex (▼), MV2 (■), and the MV2–DLC2 complex (●) as functions of the monomer fraction ( $f_M$ ). Solid lines represent nonlinear curve fitting for a two-state transition using eqs 1–3 (see the Materials and Methods). Observed melting temperatures are 20.9, 28.2, 36, and 41.1 °C for M11, the M11–DLC2 complex, MV2, and the MV2–DLC2 complex, respectively. The inset of C shows the concentration dependence of MV2 as followed by molar ellipticity changes at 222 nm and 37 °C. The solid line is fitted to a two-state transition with a calculated dissociation constant of 17  $\mu$ M. For clarity, not all data points are illustrated. (D) Thermal unfolding profiles of M11 $\Delta$ B (▼), the complex of M11 $\Delta$ B and DLC2 (▲), MV2 (■), the complex of MV2 and DLC2 (●), and DLC2 alone (◆). Protein samples (16  $\mu$ M) were heated at a constant 1 °C/min rate, and ellipticity was monitored at 222 nm.

dimer without DLC2 ( $K_d = 29 \mu$ M), which is stabilized  $\sim 15$  times in the presence of DLC2 ( $K_d = 2 \mu$ M). M11 weakly dimerizes at 25 °C even in complex with DLC2 ( $K_d = 5.5 \mu$ M). Table 1 also shows that the presence of DLC2 increased the concentration-independent melting temperatures ( $T_m$ ) of both M11 and MV2 by  $\sim 7$  °C. The dissociation constant of MV2 was also determined at 37 °C from the concentration dependence of its ellipticity at 222 nm (inset of Figure 7C). Data fitting assuming a simple monomer–dimer transition resulted in  $K_d = 17 \mu$ M, which is in good agreement with the value calculated from the temperature denaturation experiment.

The M3 construct, the isolated segment between the medial and distal coiled-coil domains, showed a strong minimum at 200 nm and a weak signal at 222 nm, representing a primarily unfolded structure. The addition of 50% TFE increased the 222 nm signal and shifted the 200 nm signal

to 208 nm, typical of  $\alpha$ -helix formation (Figure 7B). The addition of DLC2 shifted the spectrum to show double minima at 222 and 206 nm. Analysis of the spectrum indicated a  $\sim 10\%$  increase in helical content, i.e., some gain in structure upon DLC2 binding ( $\sim 8$  residues folded into the  $\alpha$  helix). Thermal denaturation of M3 did not show any cooperative transition. The M3–DLC2 complex showed a broad, gradual thermal unfolding transition ( $T_{\text{mobs}}$  was difficult to determine but is in the range of 20–25 °C). A highly disordered structure of the M3 construct was also suggested by its <sup>1</sup>H NMR spectrum (data not shown). On the basis of the above results, it appears that binding of DLC2 is accompanied by a considerable increase in stability and a moderate increase in the ordered structure of the myoVa tail domains.

*Mapping the MyoVa Binding Site on DLC2 by Peptide Competition Assay and NMR Spectroscopy.* To find out

Table 1: Thermodynamic Parameters for Unfolding of Various Myosin V Constructs (16  $\mu\text{M}$  Each) Observed by CD Spectroscopy<sup>a</sup>

	$T_{\text{mobs}}$ (°C)	$\Delta H_V$ (kJ/mol)	$T_m$ ( $\Delta G=0$ ) (°C)	$K_d$ (25 °C) ( $\mu\text{M}$ )	$K_d$ (37 °C) ( $\mu\text{M}$ )
M11	20.9	220	62.3	53	>1000
M11 plus DLC	28.2	228	70.0	6	213
MV2	36.0	402	59.3	0.03	29 (17) <sup>b</sup>
MV2 plus DLC	41.1	384	66.5	0.004	2
M2	36.3	366	62.5	0.06	13
MV2 (4 $\mu\text{M}$ )	34.8	450	57.7		
MV2 (64 $\mu\text{M}$ )	38.6	379	59.3		

<sup>a</sup> Apparent melting temperature ( $T_{\text{mobs}}$ ), the melting temperature at  $\Delta G = 0$  ( $T_m$  ( $\Delta G=0$ )), van't Hoff enthalpy of denaturation, and dissociation/unfolding constants ( $K_d$ ) were determined from the temperature dependence of ellipticity at 222 nm, assuming a two-state monomer-dimer transition and using equations detailed in the Materials and Methods. Errors of  $T_m$ ,  $\Delta H_V$ , and  $K_d$  are approximately  $\pm 0.2$  °C,  $\pm 5$  kJ/mol, and  $\pm 10\%$ , respectively. There was no concentration dependence of the  $T_m$  values evaluated at  $\Delta G = 0$ . The average  $T_m$  of MV2 at equilibrium was  $58.7 \pm 0.7$  °C over a range of 4–64  $\mu\text{M}$ . <sup>b</sup> Determined from the concentration dependence of ellipticity at 222 nm.

whether the myoVa binding site on DLC2 is the same as that for the other binding partners, we performed a peptide competition experiment. The GST–M7–DLC2 complex-bound glutathione Sepharose beads were titrated with increasing amounts of a DLC-binding nNOS peptide (EMKDTGIQVDRL). The peptide was able to disrupt the interaction of GST–M7 with DLC2 in a dose-dependent manner (Figure 8A). The fact that the nNOS peptide was able to compete with the myoVa fragment manifests that they share the same binding site on the surface of DLC2.

The titration of <sup>15</sup>N-labeled DLC2 with a 15 residue nonlabeled myoVa peptide (IQPKDDKNTMTDSTI) was also monitored by 2D <sup>1</sup>H-<sup>15</sup>N HSQC NMR measurements (Figure 8B). The HSQC spectrum of human DLC2 clearly resembles the one obtained by Day et al. (35). Already, at low peptide concentrations, two sets of peaks appeared, with one set belonging to the apo DLC2 and the other belonging to the complexed form. As the amount of the peptide increased, the intensity of the free enzyme peak for the corresponding amino acid residue decreased, while the peak belonging to the bounded residue increased in intensity. This is in accordance with a slow exchange between the two forms on the NMR time scale. Careful integration of a few selected distanced and well-resolved peaks (Asp37, Gly59, Gly63, and Gly79) led to the calculation of a  $K_d \sim 30$   $\mu\text{M}$  for the bound peptide. The titration experiment showed a 1:1 DLC2 chain/peptide ratio at the saturation point. Binding sites on DLC2 can be detected by calculating the variation of individual chemical shifts upon complex formation. Those residues that possess the most accentuated shifts are the ones involved in binding. The value is defined as

$$\Delta_{\text{ppm}} = \sqrt{(\Delta\delta_{\text{HN}})^2 + (\Delta\delta_{\text{N}}\alpha_{\text{N}})^2}$$

where  $\alpha_{\text{N}}$  is a scaling factor = 0.17.

Significant  $\Delta_{\text{ppm}}$  shifts were observed for the Asp37, Gly59, Asn61, Phe62, Gly63, Gly79, Ser64, Lys71, and Lys36 peaks (Figure 8C), residues that reside at the surface groove of the DLC2. Because no measurements were performed on the <sup>13</sup>C,<sup>15</sup>N-labeled DLC2–myoVa peptide complex, the position of several residues in the complex is

ambiguous. However, information obtained from the available data set clearly indicated that the previously identified ligand binding site of DLC2 (35) is involved in the interaction with myoVa as well. The addition of excess nNOS peptide to the DLC2–myoVa peptide complex shifted the HSQC spectrum to a new pattern, further indicating that the myoVa peptide binds to a surface on DLC2 shared by its other known partners.

*Docking of a MyoVa Peptide on the Binding Groove of DLC2.* To learn more about the binding mode of the myoVa peptide to DLC2, molecular docking simulation studies were performed (59). A control docking procedure adequately reproduced the binding geometry of the ligand Bim peptide MSCDKSTQT known from NMR structure determination (see the Materials and Methods for details). Docking of a 10 residue myoVa peptide (Ac-PKDDKNTMTD-NMe) resulted in a complex where the peptide is bound firmly to the target binding surface groove of DLC2 (Figure 9). When the docking energies of the above myoVa-binding peptide were compared with another peptide lacking exon B (Ac-QPKNTMTD-NMe), their relative binding strengths to DLC2 were estimated. The Ac-PKDDKNTMTD-NMe peptide has a significantly higher affinity to DLC2 ( $\sim 12.5$ – $25$  kJ/mol) than the Ac-QPKNTMTD-NMe peptide. Interestingly, while the Bim peptide forms eight hydrogen bonds and one salt bridge with DLC2, the backbone of the Ac-PKDDKNTMTD-NMe peptide is involved in only four hydrogen bonds. The Bim peptide binds to the target-accepting groove of DLC2 as an antiparallel  $\beta$  strand extending the mixed  $\beta$  sheet that forms the dimer interface. In the docked structure, the myoVa peptide does not form a  $\beta$  strand along its entire length; only a short antiparallel  $\beta$  structure is apparent comprising exon B and the loop connecting the 3rd and 4th  $\beta$  strands of the DLC2 monomer. The rest of the peptide sits at the bottom of the groove making several hydrophobic interactions. There are numerous interactions present between the side chains of the myoVa peptide and the DLC binding crevice. Side-chain interactions of exon B residues could strongly contribute to the binding affinity of myoVa to DLC; Asp1284 and Asp1285 are hydrogen-bonded to Thr70 and Tyr65, respectively, and Lys1286 forms a salt bridge with Asp12 in the docked structure.

## DISCUSSION

*Exon B of the MyoVa Tail Is an Essential Part of the DLC Binding Site.* In this study, we have narrowed the binding site in human myoVa by direct solution binding assays to a  $\sim 15$  residue segment (Ile1280–Ile1294) localized within a noncoiled-coil domain flanked by predicted coiled-coil domains. Because this domain (Pro1235–Arg1320) binds DLC2, we henceforth call it the DLC2 binding domain (DBD). The binding region contains three residues, coded by the alternatively spliced exon B (AspAspLys). Removal of exon B eliminates DLC binding, also affirmed by cotransfection experiments.

The tail region of myoVa is alternatively spliced at three exons. Exons B, D, and F are combinatorically included or excluded from the expressed heavy chain, providing at least six isoforms that could have specific functions (16). Our results establish a function for the 3 residue long exon B, forming an essential part of the binding site for the

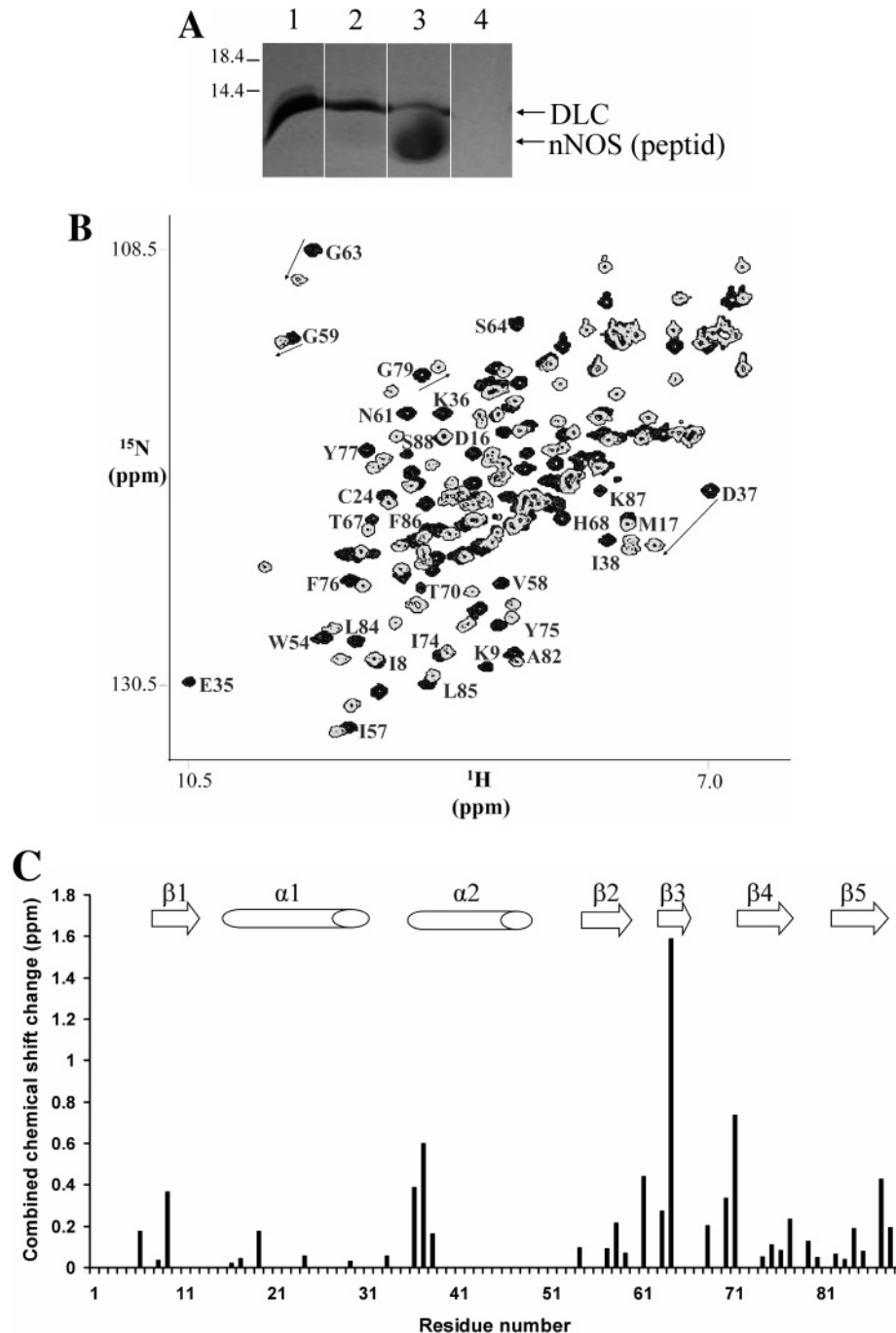


FIGURE 8: Mapping of the myoVa binding site on DLC2 by (A) the peptide competition assay and (B) NMR spectroscopy. (A) GST-M7-DLC2 complex bound to glutathion-Sepharose beads was mixed in succession with  $1\times$ ,  $10\times$ , and  $100\times$  molar excess of a DLC2-binding peptide of nNOS (EMKDTGIQVDRL), respectively, in PBS containing  $\beta$ -ME. After 30 min of incubation at  $25^\circ\text{C}$ , the supernatants were loaded on gels (lanes 1–3). The elution fraction from the glutathion beads after incubation with the nNOS peptide shows no remaining DLC2 (lane 4). All fractions were resolved by a 15% tricine SDS-PAGE. Note that the nNOS peptide is visible on the gel only at a high concentration (lane 3) (B) Superposition of  $^1\text{H}$ - $^{15}\text{N}$  HSQC spectra of free DLC2 (black) and its saturated complex with a 15-residue DLC-binding peptide of myoVa (IQPKDDKNTMTDSTI) (gray). Assignments of a few amino acids from the free DLC2 are labeled with single-letter residue name and number. Arrows indicate a chemical shift in the complexed form. (C) Histogram showing the chemical-shift differences between amine resonances of the free and bound DLC2 complex induced by ligand binding. Chemical-shift differences were calculated as defined:  $\Delta_{\text{ppm}} = \sqrt{(\Delta\delta_{\text{HN}})^2 + (\Delta\delta_{\text{N}}\alpha_{\text{N}})^2}$ , where  $\Delta\delta_{\text{HN}}$  and  $\Delta\delta_{\text{N}}$  are the chemical-shift changes of the HN and N resonances, respectively, and  $\alpha_{\text{N}}$  is a scaling factor = 0.17. The position of the secondary-structure elements of DLC2 is shown above the histogram as determined in ref 35.

tail-associated DLC in the mainly brain-specific splice form of myoVa. Although exon D closely follows the identified DLC binding sequence, it is not involved in the binding. The major role of the alternative tail exon-coded sequences of myoVa appears to provide specific binding surfaces to different interacting partners (16). Interestingly, the other two

mammalian myosin V paralogue genes, MYO5B and MYO5C, do not contain exon B; thus, their protein products lack the tail-associated light chain. Sequence analysis of all of the known myoVa genes points to the appearance of these three residue insertions in the vertebrate lineage (results are available from the authors by request). A comparison of the

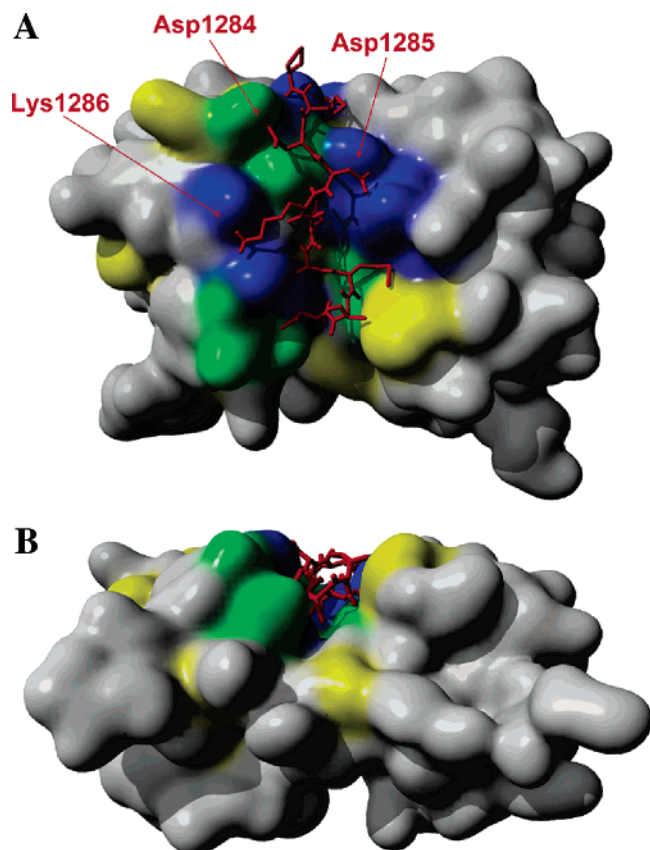


FIGURE 9: Docking of a myoVa peptide to DLC2. The myoVa binding peptide Ac-PKDDKNTMTD-NMe (red sticks) was docked using AutoDock 3.0 after energy minimization of the average NMR structure of the DLC1–Bim complex (PDB 1F95). The molecular surface of DLC2 is shown. Putative binding site residues on DLC2 are highlighted: green, identified by both docking and a chemical shift of amide resonances in  $^1\text{H}$ - $^{15}\text{N}$  HSQC spectra of the complex (Figure 8); blue, identified by docking only; and yellow, identified by NMR only. The position of exon B residues (AspAspLys) is indicated. (A) Target peptide binding groove is shown from above (A) and rotated  $90^\circ$  (B). Only one of the binding peptides is shown on the homodimeric DLC2. The figure was made by YASARA and rendered by POV-Ray.

known vertebrate exon B sequences shows that the third residue is invariably Lys, while the first and second residues must be negatively charged and could be either Asp or Glu.

During the course of the present study, Lajoix et al. (67) has reported the identification of a DLC1 binding site on chicken myoVa using an immobilized peptide-scanning technique; the shortest peptide found to bind to DLC1 was EDKNTMTD. Surprisingly, the same method in another laboratory failed to identify a DLC binding site (41). The discrepancy might be due to the fact that the immobilized short peptide binds only weakly to DLC. Indeed, we found by NMR titration that the affinity of a similar short synthetic peptide of myoVa to DLC is weak ( $K_d \sim 30 \mu\text{M}$ ).

*DLC Acts as a “Molecular Glue” To Stabilize the Medial and Distal Coiled-Coil Domains of MyoVa.* Spectroscopy measurements indicated that the recombinant monomeric DBD does not fold into a stable three-dimensional structure but forms an intrinsically unfolded domain (68) that acquires some helical structure in the presence of bound DLC2. However, we cannot rule that DBD is partially stabilized in its natural sequence environment by the neighboring coiled-coil domains. More strikingly, binding of DLC2 is able to

stabilize not only its immediate binding domain but also the flanking coiled-coil domains. Without DLC, the medial and distal coiled-coil segments are only marginally stable at physiologically relevant temperature (at  $37^\circ\text{C}$ ,  $\sim 20 \mu\text{M}$ ). Sequence analysis of the medial and distal coiled-coils could, at least, partially explain their low stability. For their length (about five continuous heptade repeats at each end of DBD), they contain many destabilizing polar residues at the core “a” and “d” positions (9 of 21). Such a weak coiled-coil segment has recently been described in the crystal structure of a conventional myosin tail (69). It is conceivable that the heavy chains of myoVa tails without the bound DLC2 do not form dimers beyond the PEST site. Assuming that the intracellular protein concentration is  $150\text{--}200 \text{ mg/mL}$  (70) and that myoVa represents about 1% of the total protein, its average concentration is in the range of a few micromolar. On the basis of these numbers, one can estimate that only  $\sim 5\%$  of MV2 forms dimers at  $37^\circ\text{C}$ . The full-length myosin is likely dimeric under these conditions, but the heavy chains in the distal tail could be separated, affecting the function of the motor protein. Binding of DLC2 to the tail stabilizes both the medial and distal coiled-coils against at least 1 order of magnitude differences in  $K_d$  values at physiological temperatures. An increase in molar ellipticities at 222 nm accompanied by an increase in the ratio of ellipticities at 222 and 208 nm indicates an increase in higher ordered helical structures (i.e., coiled-coil) and suggests that DLC2 acts remotely by stabilizing the flanking coiled-coil domains. In light of these results, one can wonder about the mechanism of such an allosteric effect of DLC2 binding. A plausible explanation might be that one DLC2 dimer is able to cross-link two DBDs and thus, by physically bringing closer the two heavy chains, stabilizes the attached coiled-coils. Interestingly, the only detailed interaction study between DLC1 and two target proteins, dynein intermediate chain and the *Drosophila* swallow protein (30, 71), suggested a similar stabilizing role of DLC1. It binds to a partially disordered region of the dynein intermediate chain, which gains structure only upon DLC1 binding (71), and it promotes the assembly of the coiled-coil domain of the swallow protein flanking the DLC1 binding site (30). These findings correspond exactly to the features deduced in this work from studying the formation of the DLC2–myoVa complex. Our results strengthen the conclusion of Barbar et al. (30, 71) that DLC could promote the assembly of protein complexes as a “molecular glue” by increasing the ordered structure of its interacting partners.

*Structural/Functional Implication of the DLC2–MyoVa Interaction.* It is clear from our peptide competition and NMR spectroscopic and docking studies that myoVa is able to bind to the same surface groove of DLC2 as other known binding partners. The crystal structure of a 13 residue peptide fragment from nNOS bound to DLC1 showed that the peptide binding site is a deep hydrophobic cleft formed by strands  $\beta_3$ ,  $\beta_4$ , and  $\beta_5$  from one protomer and  $\alpha_2$  from the other. The peptide interacts extensively, via backbone hydrogen bonds and side-chain hydrophobic and hydrophilic interactions, with strand  $\beta_3$  in an antiparallel manner, extending the central  $\beta$  sheet of DLC1 to six antiparallel  $\beta$  strands (43, 45). The same binding characteristics were obtained by NMR spectroscopy of Bim and Bmf binding to DLC1 and DLC2, respectively (35, 45). On the basis of the

residues implicated in binding by NMR and docking studies, even if sharing a common binding groove, myoVa may behave somewhat differently. The docking model shows that the myoVa peptide does not form a continuous  $\beta$  strand but only a short one involving the three exon B residues. A more detailed comparison of the known structures is precluded by the relatively large rmsd of the docking model, owing to the large number of atoms involved in the simulation. How is the DLC binding sequence of myoVa related to other DLC binding sites? Previously, biochemical and mutational analysis of many DLC partners identified two consensus sequences (K/R)XTQT and G(I/V)QV(D/E) (41). When all known DLC binding sequences were compared, Lajoix et al. (67) found DKGTQT being the most frequent binding motif among diverse sequences. The promiscuous nature of the partner binding site of DLCs is thought to be based on the conformational breathing of its binding groove (45, 67). Substitution analysis indicated that the Gln, flanked by two hydrophobic residues, is the most critical residue for determining the binding strength of many DLC partners. The only DLC binding sequence where this Gln is substituted by Met is myoVa. This Gln caps  $\alpha$  helix 2, while the flanking residues are bound to  $\beta$  strands 2 and 3 in the hydrophobic groove. Missing interactions with Gln could contribute to the weaker affinity of the myoVa peptide to DLC2 compared to other binding peptides. The replacement of the corresponding Met to Gln in the synthetic binding peptide indeed resulted in strongly increased binding (67).  $K_d$  of the myoVa peptide to DLC2 was found to be  $\sim 30 \mu\text{M}$ ; however, binding of the longer myoVa constructs (namely, of MV2) has an estimated affinity of  $\sim 0.5 \mu\text{M}$ , suggesting additional interaction surfaces between the two proteins. Work is in progress to investigate the kinetic and thermodynamic details of the binding process between DLC2 and myoVa.

In regard to the function of DLCs as subunits of motor proteins, previous suggestions were stabilizing, cargo binding, and/or some regulatory roles (7, 34). Our results are consistent with a role as a molecular glue (see above). When exon B and its associated DLC2 were brought in close proximity to the two heavy chains and hence stabilized the medial and proximal coiled-coil domains, they could form or expose binding sites for additional regulatory proteins/cargos and/or could provide the globular tail domain with extra cargo-interacting specificity as suggested for the other two alternative tail exons (16). If exon B and DLC2 have this property, then myoVa isoforms with and without exon B could have specific roles. The stability of the medial coiled-coil domain indeed seems to be critical to the myoVa function; the mutation of Leu1211 to a Gln (a core d position in the medial coiled-coil domain) was found in a *dilute* mutant mouse (11). Another possible role of DLC2 could be its involvement in the regulation of the motor activity. The current model of regulation suggests that full-length myoVa in the presence of low  $\text{Ca}^{+2}$  can adopt an inhibited compact conformation, where the globular tail domains are folded back to the two heads. Cargo binding or elevated  $\text{Ca}^{+2}$  would unlock the motor by independent pathways (17–20). The tail light chain, bound to the flexible exon B containing the domain between the medial and distal coiled-coils, would be in an ideal position to affect the inhibitory folded state. On early electron microscopy (EM) pictures of brain-isolated myoVa, Cheney et al. (8) observed molecules with the

globular tail domain superimposed on a tail region that could easily be DBD with bound DLC2. If such an interaction exists, it could provide an additional level of regulation in class V myosins.

Finally, the key question remains whether DLC2 (or DLC1 on the dynein motor) could act as a cargo-binding adaptor protein or not? In this respect, the symmetric nature of the partner binding groove of DLC raises some concern if the myoVa heavy chains and the dynein intermediate chains occupy both binding grooves of DLC. As a consequence, one of the motor chains must be displaced by the cargo for the cargo to bind. This so-called cargo-binding problem could be solved if the binding sites are asymmetric and/or binding to the dimeric motor displays negative cooperativity. A similar situation exists in Tctex1, another DLC (72, 73). For this structural homologue of DLC, the binding site to the dynein intermediate chain is distinct from the potential cargo binding site (74), allowing for the binding of rhodopsin cargo without disrupting the Tctex1–motor interaction. In the case of the DLC2–myoVa complex, our results suggest that the DLC dimer brings together the two heavy chains by binding simultaneously to them. These results are more consistent with a symmetric binding model; however, we cannot rule out that the two interfaces between the DLC dimer and the exon B containing heavy chains are not fully identical and somehow allow for the simultaneous binding of DLC2 to the heavy chain and the cargo protein. Further structural and kinetic studies are required to understand the detailed mechanism of cargo binding to the assembled myoVa motor complex.

## ACKNOWLEDGMENT

We are grateful to Katalin Kurucz-Váradí for her excellent technical assistance, Erika Kovács for making the constructs for the transfection experiments, Dr. András Pathy for peptide synthesis and sequencing, and Dr. Péter Závodszy for allowing us to use his spectropolarimeter. We thank Dr. M. G. Hinds for providing his sequence assignment of the HSQC spectra of DLC2 and Dr. Rodriguez-Crespo for providing the DLC-binding nNOS peptide. We also thank L. Farkas, J. Kardos, M. Kovács, and J. Tóth for their helpful discussions and comments.

## REFERENCES

1. Reck-Peterson, S. L., Provance, D. W., Jr., Mooseker, M. S., and Mercer, J. A. (2000) Class V myosins, *Biochim. Biophys. Acta* 1496, 36–51.
2. Mehta, A. D., Rock, R. S., Rief, M., Spudich, J. A., Mooseker, M. S., and Cheney, R. E. (1999) Myosin-V is a processive actin-based motor, *Nature* 400, 590–593.
3. Rief, M., Rock, R. S., Mehta, A. D., Mooseker, M. S., Cheney, R. E., and Spudich, J. A. (2000) Myosin-V stepping kinetics: A molecular model for processivity, *Proc. Natl. Acad. Sci. U.S.A.* 97, 9482–9486.
4. Mercer, J. A., Seperack, P. K., Strobel, M. C., Copeland, N. G., and Jenkins, N. A. (1991) Novel myosin heavy chain encoded by murine dilute coat colour locus, *Nature* 349, 709–713.
5. Pastural, E., Barrat, F. J., Dufourcq-Lagelouse, R., Certain, S., Sanal, O., Jabado, N., Seger, R., Griscelli, C., Fischer, A., and de Saint Basile, G. (1997) Griscelli disease maps to chromosome 15q21 and is associated with mutations in the myosin-Va gene, *Nat. Genet.* 16, 289–292.
6. Espindola, F. S., Suter, D. M., Partata, L. B., Cao, T., Wolenski, J. S., Cheney, R. E., King, S. M., and Mooseker, M. S. (2000) The light chain composition of chicken brain myosin-Va: Calm-

- odulin, myosin-II essential light chains, and 8-kDa dynein light chain/PIN, *Cell Motil. Cytoskeleton* 47, 269–281.
7. Pfister, K. K., Shah, P. R., Hummerich, H., Russ, A., Cotton, J., Annuar, A. A., King, S. M., and Fisher, E. M. (2006) Genetic analysis of the cytoplasmic dynein subunit families, *PLoS Genet.* 2, e1.
  8. Cheney, R. E., O'Shea, M. K., Heuser, J. E., Coelho, M. V., Wolenski, J. S., Espreafico, E. M., Forscher, P., Larson, R. E., and Mooseker, M. S. (1993) Brain myosin-V is a two-headed unconventional myosin with motor activity, *Cell* 75, 13–23.
  9. Pashkova, N., Jin, Y., Ramaswamy, S., and Weisman, L. S. (2006) Structural basis for myosin V discrimination between distinct cargoes, *EMBO J.* 25, 693–700.
  10. Seperack, P. K., Mercer, J. A., Strobel, M. C., Copeland, N. G., and Jenkins, N. A. (1995) Retroviral sequences located within an intron of the dilute gene alter dilute expression in a tissue-specific manner, *EMBO J.* 14, 2326–2332.
  11. Huang, J. D., Mermell, V., Strobel, M. C., Russell, L. B., Mooseker, M. S., Copeland, N. G., and Jenkins, N. A. (1998) Molecular genetic dissection of mouse unconventional myosin-VA: Tail region mutations, *Genetics* 148, 1963–1972.
  12. Lambert, J., Naeyaert, J. M., Callens, T., De Paepe, A., and Messiaen, L. (1998) Human myosin V gene produces different transcripts in a cell type-specific manner, *Biochem. Biophys. Res. Commun.* 252, 329–333.
  13. Fukuda, M., Kuroda, T. S., and Mikoshiba, K. (2002) Slac2-a/melanophilin, the missing link between Rab27 and myosin Va: Implications of a tripartite protein complex for melanosome transport, *J. Biol. Chem.* 277, 12432–12436.
  14. Strom, M., Hume, A. N., Tarafder, A. K., Barkagianni, E., and Seabra, M. C. (2002) A family of Rab27-binding proteins. Melanophilin links Rab27a and myosin Va function in melanosome transport, *J. Biol. Chem.* 277, 25423–25430.
  15. Wu, X. S., Rao, K., Zhang, H., Wang, F., Sellers, J. R., Matesic, L. E., Copeland, N. G., Jenkins, N. A., and Hammer, J. A., III (2002) Identification of an organelle receptor for myosin-Va, *Nat. Cell Biol.* 4, 271–278.
  16. Westbroek, W., Lambert, J., Bahadoran, P., Busca, R., Herteleer, M. C., Smit, N., Mommaas, M., Ballotti, R., and Naeyaert, J. M. (2003) Interactions of human myosin Va isoforms, endogenously expressed in human melanocytes, are tightly regulated by the tail domain, *J. Invest. Dermatol.* 120, 465–475.
  17. Kremmentsov, D. N., Kremmentsova, E. B., and Trybus, K. M. (2004) Myosin V: Regulation by calcium, calmodulin, and the tail domain, *J. Cell Biol.* 164, 877–886.
  18. Li, X.-d., Mabuchi, K., Ikebe, R., and Ikebe, M. (2004) Ca<sup>2+</sup>-Induced activation of ATPase activity of myosin Va is accompanied with a large conformational change, *Biochem. Biophys. Res. Commun.* 315, 538.
  19. Wang, F., Thirumurugan, K., Stafford, W. F., Hammer, J. A., III, Knight, P. J., and Sellers, J. R. (2004) Regulated conformation of myosin V, *J. Biol. Chem.* 279, 2333–2336.
  20. Liu, J., Taylor, D. W., Kremmentsova, E. B., Trybus, K. M., and Taylor, K. A. (2006) Three-dimensional structure of the myosin V inhibited state by cryoelectron tomography, *Nature* 442, 208–211.
  21. Thirumurugan, K., Sakamoto, T., Hammer, J. A., III, Sellers, J. R., and Knight, P. J. (2006) The cargo-binding domain regulates structure and activity of myosin V, *Nature* 442, 212–215.
  22. King, S. M. (2000) The dynein microtubule motor, *Biochim. Biophys. Acta* 1496, 60–75.
  23. King, S. M., and Patel-King, R. S. (1995) The M<sub>r</sub> = 8,000 and 11,000 outer arm dynein light chains from *Chlamydomonas* flagella have cytoplasmic homologues, *J. Biol. Chem.* 270, 11445–11452.
  24. Lo, K. W., Naisbitt, S., Fan, J. S., Sheng, M., and Zhang, M. (2001) The 8-kDa dynein light chain binds to its targets via a conserved (K/R)XTQT motif, *J. Biol. Chem.* 276, 14059–14066.
  25. Wilson, M. J., Salata, M. W., Susalka, S. J., and Pfister, K. K. (2001) Light chains of mammalian cytoplasmic dynein: Identification and characterization of a family of LC8 light chains, *Cell Motil. Cytoskeleton* 49, 229–240.
  26. Jaffrey, S. R., and Snyder, S. H. (1996) PIN: An associated protein inhibitor of neuronal nitric oxide synthase, *Science* 274, 774–777.
  27. Rodriguez-Crespo, I., Straub, W., Gavilanes, F., and Ortiz de Montellano, P. R. (1998) Binding of dynein light chain (PIN) to neuronal nitric oxide synthase in the absence of inhibition, *Arch. Biochem. Biophys.* 359, 297–304.
  28. Crepieux, P., Kwon, H., Leclerc, N., Spencer, W., Richard, S., Lin, R., and Hiscott, J. (1997) IκBα physically interacts with a cytoskeleton-associated protein through its signal response domain, *Mol. Cell Biol.* 17, 7375–7385.
  29. Schnorrer, F., Bohmann, K., and Nusslein-Volhard, C. (2000) The molecular motor dynein is involved in targeting swallow and bicoid RNA to the anterior pole of *Drosophila* oocytes, *Nat. Cell Biol.* 2, 185–190.
  30. Wang, L., Hare, M., Hays, T. S., and Barbar, E. (2004) Dynein light chain LC8 promotes assembly of the coiled-coil domain of swallow protein, *Biochemistry* 43, 4611–4620.
  31. Epstein, E., Sela-Brown, A., Ringel, I., Kilav, R., King, S. M., Benashski, S. E., Yisraeli, J. K., Silver, J., and Naveh-Manly, T. (2000) Dynein light chain binding to a 3'-untranslated sequence mediates parathyroid hormone mRNA association with microtubules, *J. Clin. Invest.* 105, 505–512.
  32. Fuhrmann, J. C., Kins, S., Rostaing, P., El Far, O., Kirsch, J., Sheng, M., Triller, A., Betz, H., and Kneussel, M. (2002) Gephyrin interacts with dynein light chains 1 and 2, components of motor protein complexes, *J. Neurosci.* 22, 5393–5402.
  33. Haraguchi, K., Satoh, K., Yanai, H., Hamada, F., Kawabuchi, M., and Akiyama, T. (2000) The hDLG-associated protein DAP interacts with dynein light chain and neuronal nitric oxide synthase, *Genes Cells* 5, 905–911.
  34. Naisbitt, S., Valtschanoff, J., Allison, D. W., Sala, C., Kim, E., Craig, A. M., Weinberg, R. J., and Sheng, M. (2000) Interaction of the postsynaptic density-95/guanylate kinase domain-associated protein complex with a light chain of myosin-V and dynein, *J. Neurosci.* 20, 4524–4534.
  35. Day, C. L., Puthalakath, H., Skea, G., Strasser, A., Barsukov, I., Lian, L. Y., Huang, D. C., and Hinds, M. G. (2004) Localization of dynein light chains 1 and 2 and their pro-apoptotic ligands, *Biochem. J.* 377, 597–605.
  36. Puthalakath, H., Villunger, A., O'Reilly, L. A., Beaumont, J. G., Coultas, L., Cheney, R. E., Huang, D. C., and Strasser, A. (2001) Bmf: A proapoptotic BH3-only protein regulated by interaction with the myosin V actin motor complex, activated by anoikis, *Science* 293, 1829–1832.
  37. Lo, K. W., Kan, H. M., Chan, L. N., Xu, W. G., Wang, K. P., Wu, Z., Sheng, M., and Zhang, M. (2005) The 8-kDa dynein light chain binds to p53-binding protein 1 and mediates DNA damage-induced p53 nuclear accumulation, *J. Biol. Chem.* 280, 8172–8179.
  38. Martinez-Moreno, M., Navarro-Lerida, I., Roncal, F., Albar, J. P., Alonso, C., Gavilanes, F., and Rodriguez-Crespo, I. (2003) Recognition of novel viral sequences that associate with the dynein light chain LC8 identified through a pepscan technique, *FEBS Lett.* 544, 262–267.
  39. Poisson, N., Real, E., Gaudin, Y., Vaney, M. C., King, S., Jacob, Y., Tordo, N., and Blondel, D. (2001) Molecular basis for the interaction between rabies virus phosphoprotein P and the dynein light chain LC8: Dissociation of dynein-binding properties and transcriptional functionality of P, *J. Gen. Virol.* 82, 2691–2696.
  40. Navarro-Lerida, I., Martinez Moreno, M., Roncal, F., Gavilanes, F., Albar, J. P., and Rodriguez-Crespo, I. (2004) Proteomic identification of brain proteins that interact with dynein light chain LC8, *Proteomics* 4, 339–346.
  41. Rodriguez-Crespo, I., Yelamos, B., Roncal, F., Albar, J. P., Ortiz de Montellano, P. R., and Gavilanes, F. (2001) Identification of novel cellular proteins that bind to the LC8 dynein light chain using a pepscan technique, *FEBS Lett.* 503, 135–141.
  42. Dick, T., Ray, K., Salz, H. K., and Chia, W. (1996) Cytoplasmic dynein (ddlc1) mutations cause morphogenetic defects and apoptotic cell death in *Drosophila melanogaster*, *Mol. Cell Biol.* 16, 1966–1977.
  43. Liang, J., Jaffrey, S. R., Guo, W., Snyder, S. H., and Clardy, J. (1999) Structure of the PIN/LC8 dimer with a bound peptide, *Nat. Struct. Biol.* 6, 735–740.
  44. Vadlamudi, R. K., Bagheri-Yarmand, R., Yang, Z., Balasenthil, S., Nguyen, D., Sahin, A. A., den Hollander, P., and Kumar, R. (2004) Dynein light chain 1, a p21-activated kinase 1-interacting substrate, promotes cancerous phenotypes, *Cancer Cell* 5, 575–585.
  45. Fan, J., Zhang, Q., Tochio, H., Li, M., and Zhang, M. (2001) Structural basis of diverse sequence-dependent target recognition by the 8 kDa dynein light chain, *J. Mol. Biol.* 306, 97–108.
  46. Hódi, Z. N., A., Hetényi, Cs., Bodor, A., Perczel, A., and Nyitrai, L. (2005) Alternatively spliced exon B of myosin Va is essential

- for binding of the tail light chain shared by dynein, *J. Muscle Res. Cell Motil.* 26, 73.
47. Pace, C. N., Vajdos, F., Fee, L., Grimsley, G., and Gray, T. (1995) How to measure and predict the molar absorption coefficient of a protein, *Protein Sci.* 4, 2411–2423.
48. Stoscheck, C. M. (1990) Quantitation of protein, *Methods Enzymol.* 182, 50–68.
49. Schagger, H., and von Jagow, G. (1987) Tricine–sodium dodecyl sulfate–polyacrylamide gel electrophoresis for the separation of proteins in the range from 1 to 100 kDa, *Anal. Biochem.* 166, 368–379.
50. Schlett, K., and Madarasz, E. (1997) Retinoic acid induced neural differentiation in a neuroectodermal cell line immortalized by p53 deficiency, *J. Neurosci. Res.* 47, 405–415.
51. Li, X., Romero, P., Rani, M., Dunker, A. K., and Obradovic, Z. (1999) Predicting protein disorder for N-, C-, and internal regions, *Genome Inf. Ser. Workshop Genome Inf.* 10, 30–40.
52. Linding, R., Russell, R. B., Neduva, V., and Gibson, T. J. (2003) GlobPlot: Exploring protein sequences for globularity and disorder, *Nucleic Acids Res.* 31, 3701–3708.
53. Rost, B., and Sander, C. (1993) Prediction of protein secondary structure at better than 70% accuracy, *J. Mol. Biol.* 232, 584–599.
54. Greenfield, N. J., Montelione, G. T., Farid, R. S., and Hitchcock-DeGregori, S. E. (1998) The structure of the N-terminus of striated muscle  $\alpha$ -tropomyosin in a chimeric peptide: Nuclear magnetic resonance structure and circular dichroism studies, *Biochemistry* 37, 7834–7843.
55. Compton, L. A., and Johnson, W. C., Jr. (1986) Analysis of protein circular dichroism spectra for secondary structure using a simple matrix multiplication, *Anal. Biochem.* 155, 155–167.
56. Rohl, C. A., and Baldwin, R. L. (1997) Comparison of NH exchange and circular dichroism as techniques for measuring the parameters of the helix–coil transition in peptides, *Biochemistry* 36, 8435–8442.
57. Delaglio, F., Grzesiek, S., Vuister, G. W., Zhu, G., Pfeifer, J., and Bax, A. (1995) NMRPipe: A multidimensional spectral processing system based on UNIX pipes, *J. Biomol. NMR* 6, 277–293.
58. Lindahl, E., Hess, B., and van der Spoel, D. (2001) GROMACS 3.0: A package for molecular simulation and trajectory analysis, *J. Mol. Model.* 8, 306–317.
59. Morris, G. M., Goodsell, D. S., Halliday, R. S., Huey, R., Hart, W. E., Belew, R. K., Olson, A. J. (1998) Automated docking using a Lamarckian genetic algorithm and an empirical binding free energy function, *J. Comput. Chem.* 19, 1639–1662.
60. Hetenyi, C., Maran, U., Karelson, M. (2003) A comprehensive docking study on the selectivity of binding of aromatic compounds to proteins, *J. Chem. Inf. Comput. Sci.* 43, 1576–1583.
61. Fodor, K., Harmat, V., Hetenyi, C., Kardos, J., Antal, J., Perczel, A., Patthy, A., Katona, G., and Graf, L. (2005) Extended intermolecular interactions in a serine protease–canonical inhibitor complex account for strong and highly specific inhibition, *J. Mol. Biol.* 350, 156–169.
62. Espreafico, E. M., Cheney, R. E., Matteoli, M., Nascimento, A. A., De Camilli, P. V., Larson, R. E., and Mooseker, M. S. (1992) Primary structure and cellular localization of chicken brain myosin-V (p190), an unconventional myosin with calmodulin light chains, *J. Cell Biol.* 119, 1541–1557.
63. Barbar, E., Kleinman, B., Imhoff, D., Li, M., Hays, T. S., and Hare, M. (2001) Dimerization and folding of LC8, a highly conserved light chain of cytoplasmic dynein, *Biochemistry* 40, 1596–1605.
64. Lau, S. Y., Taneja, A. K., and Hodges, R. S. (1984) Synthesis of a model protein of defined secondary and quaternary structure. Effect of chain length on the stabilization and formation of two-stranded  $\alpha$ -helical coiled-coils, *J. Biol. Chem.* 259, 13253–13261.
65. Sonnichsen, F., Van Eyk, J., Hodges, R., and Sykes, B. (1992) Effect of trifluoroethanol on protein secondary structure: An NMR and CD study using a synthetic actin peptide, *Biochemistry* 31, 8790–8798.
66. Dragan, A. I., and Privalov, P. L. (2002) Unfolding of a leucine zipper is not a simple two-state transition, *J. Mol. Biol.* 321, 891–908.
67. Lajoix, A. D., Gross, R., Aknin, C., Dietz, S., Granier, C., and Laune, D. (2004) Cellulose membrane supported peptide arrays for deciphering protein–protein interaction sites: The case of PIN, a protein with multiple natural partners, *Mol. Diversity* 8, 281–290.
68. Tompa, P. (2002) Intrinsically unstructured proteins, *Trends Biochem. Sci.* 27, 527–533.
69. Li, Y., Brown, J. H., Reshetnikova, L., Blazsek, A., Farkas, L., Nyitray, L., and Cohen, C. (2003) Visualization of an unstable coiled coil from the scallop myosin rod, *Nature* 424, 341–345.
70. Guyton, A. C., and Hall, J. E. (1998) *Textbook of Medical Physiology*, WB Saunders Company, Philadelphia, PA.
71. Nyarko, A., Hare, M., Hays, T. S., and Barbar, E. (2004) The intermediate chain of cytoplasmic dynein is partially disordered and gains structure upon binding to light-chain LC8, *Biochemistry* 43, 15595–15603.
72. Williams, J. C., Xie, H., and Hendrickson, W. A. (2005) Crystal structure of dynein light chain TcTex-1, *J. Biol. Chem.* 280, 21981–21986.
73. Wu, H., Maciejewski, M. W., Takebe, S., and King, S. M. (2005) Solution structure of the Tctex1 dimer reveals a mechanism for dynein–cargo interactions, *Structure* 13, 213–223.
74. Mok, Y. K., Lo, K. W., and Zhang, M. (2001) Structure of Tctex-1 and its interaction with cytoplasmic dynein intermediate chain, *J. Biol. Chem.* 276, 14067–14074.

BI060991E